

Solution-Crystallized Organic Semiconductors with High Carrier Mobility and Air Stability

Shaohua Dong, Hongtao Zhang, Liu Yang, Meilin Bai, Yuan Yao, Hongliang Chen, Lin Gan, Tieying Yang, Hong Jiang, Shimin Hou, Lijun Wan, and Xuefeng Guo*

Organic field-effect transistors (OFETs) have continuously attracted intense research interest as a viable alternative to amorphous silicon thin-film transistors for potential applications in large-area and flexible electronics.^[1] Thanks to tremendous developments of novel high-performance organic semiconductors and device optimization,^[2] the very high field-effect mobilities of OFETs that are beyond $1 \text{ cm}^2 \text{ V}^{-1} \text{ s}^{-1}$ have been recently reported,^[3] which, however, generally required complex physical vapor or vacuum deposition techniques. To enable low-cost manufacturing, materials fabrication through simple solution processing under ambient conditions is highly desirable.^[2a-c,2e] However, the electrical properties of current OFETs fabricated with solution techniques remain inferior to those of the vacuum-deposited devices because of more defects and carrier traps in thin films and/or the instability in air. Up to now, only few examples reported such high carrier mobilities of OFETs formed from solution.^[4] Consequently, rational design

of the chemical structure of solution-processable organic semiconductors to achieve optimum molecular ordering and maximum orbital coupling that enable efficient and stable charge transport between neighboring molecules is still a big challenge for future OFET technology.^[5]

Among many organic semiconducting materials used in OFETs, oligothiophenes and polythiophenes represent a promising class of organic semiconductors for solution-processed OFETs because of their relatively straightforward synthesis and flexible structural modification.^[1a,2a,2b,2e,2i] However, defects in their solution-processed thin films and the sensitivity to photo-oxidative doping/bleaching hamper the intrinsic charge carrier transport and yield poor transistor performance (e.g., low mobility, low current on/off ratio, etc.). To remove defects and restore the device performance, we intend to modify oligothiophene backbones with strategically-placed long alkyl side-chains. This modification has two designed considerations. The first is to integrate self-healing capabilities of liquid crystals into oligothiophene molecules, which can spontaneously self-organize into highly ordered molecular stacks during thermal annealing. Only very few liquid crystalline semiconductors have been recently demonstrated with improved transistor characteristics in thin films (mobility 10^{-2} – $10^{-1} \text{ cm}^2 \text{ V}^{-1} \text{ s}^{-1}$).^[6] The second is to facilitate molecular self-assembly to form high-quality single crystals that possess essentially perfect molecular ordering ideally for charge transport. Because of the poor crystallinity oligothiophene-based single crystal transistors are not available except rare cases using fused thienoacenes.^[7] On the other hand, to impart sufficient oxidative stability to the system, we intend to employ unsubstituted quaterthiophene or pentathiophene backbones, which possess rotational freedom to some extent, for tuning effective π -conjugation. This strategy is of great value to achieve a good balance between device functionality and oxidative doping stability as previously demonstrated.^[6a-d,8] With these molecular designs taken together, we focused on alkylated oligothiophenes as active semiconductors for use in low-cost high-performance OFETs. In this study, we present two liquid crystalline oligothiophene derivatives (**1** and **2**, Scheme 1) and their OFET devices that show very high average field-effect mobility of $4.0 \text{ cm}^2 \text{ V}^{-1} \text{ s}^{-1}$ with the highest up to $6.2 \text{ cm}^2 \text{ V}^{-1} \text{ s}^{-1}$.

Figure 1a shows the UV-vis absorption spectra of compounds **1** and **2** in THF ($1 \times 10^{-5} \text{ M}$) and in annealed thin films (70 °C for **1** and 140 °C for **2** for 10 min), respectively. In dilute solution, the strongest absorption band at $\lambda_{\text{max}} = 437 \text{ nm}$ of **2** showed an obvious red-shift relative to that of **1** ($\lambda_{\text{max}} = 413 \text{ nm}$) due to the extended effective π -conjugation with the increase of thiophene units, reflecting a smaller HOMO–LUMO gap

Dr. S. Dong, H. Zhang, Y. Yao, H. Chen, L. Gan,
Prof. H. Jiang, Prof. X. Guo
Center for Nanochemistry
Beijing National Laboratory
for Molecular Sciences (BNLMS)
State Key Laboratory for Structural Chemistry
of Unstable and Stable Species, College of Chemistry
and Molecular Engineering, Peking University
Beijing 100871, PR China
E-mail: guoxf@pku.edu.cn



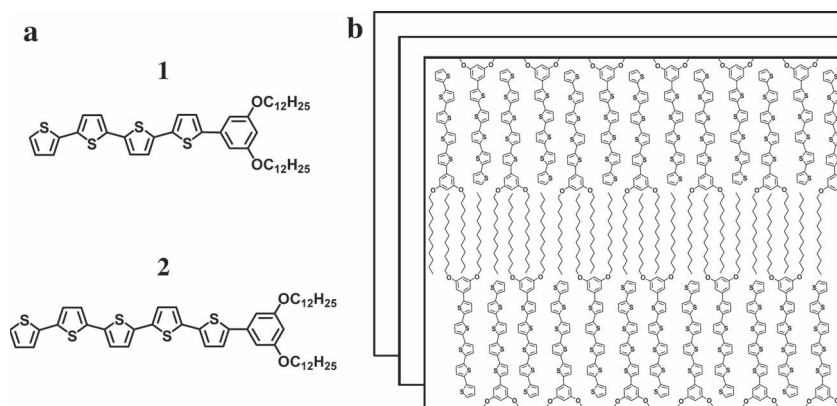
L. Yang, Prof. L. Wan
Key Laboratory of Molecular Nanostructure and Nanotechnology
Institute of Chemistry
Chinese Academy of Sciences
Beijing 100190, PR China

M. Bai, Prof. S. Hou
Key Laboratory for the Physics and Chemistry of Nanodevices
Department of Electronics
Peking University
Beijing 100871, PR China

Dr. T. Yang
Shanghai Institute of Applied Physics
Chinese Academy of Sciences
Shanghai 201204, PR China

Prof. X. Guo
Department of Advanced Materials and Nanotechnology
College of Engineering, Peking University
Beijing 100871, PR China

DOI: 10.1002/adma.201202099



Scheme 1. Molecular structures a) and proposed packing mode b) of compounds 1 and 2.

(E_g). The absorption spectra of both compounds in thin films significantly differ from those of the isolated molecules in solution. Comparison with the absorption features in solution reveals a blue-shift of the maximum, a simultaneous red-shift of the onset, and newly-formed fine peaks at lower energies. Those changes are indicative of the formation of H-aggregates with close π -stacking in a face-to-face alignment, which have been observed in crystalline oligothiophene derivatives.^[9] The strategically-positioned long alkyl side-chains can help molecules through self-assembly to achieve long-range intermolecular side-chain interdigitation in the condensed phase, thus forming lamella-like layered π -stacking structural orders as

schematically represented in Scheme 1b.^[6] In case of 2, an even larger blue-shift was observed ($\Delta\lambda = 36$ nm for 1 and 46 nm for 2, Table S1, Supporting Information), indicating the formation of better π -packing. This suggests that compound 2 might display the better device performance. The estimated E_g s from the absorption edge are ca. 2.14 eV for 1 and 2.00 eV for 2 in thin films (Table S1). These are close to that of P3HT estimated from its thin film absorption spectrum (~ 1.9 eV), suggesting their typical p-type device characteristics as discussed below.

Cyclic voltammetric (CV) studies of both compounds under nitrogen in 0.1M $\text{CH}_2\text{Cl}_2/\text{TBAPF}_6$ solutions showed the reversible oxidative peaks (Figure 1b) with the HOMO energy levels (i.e. the minus of their ionization potentials, IPs) estimated from the oxidation onset at -5.37 eV and -5.30 eV for 1 and 2, respectively. Compared with regioregular P3HT (-5.02 eV) and other fused thiophene-based polymers,^[6a,6b,6d] both 1 and 2 possess the deeper-lying HOMO energy level, thus imparting the sufficient stability against oxidative doping to themselves. This is because of the π -conjugation cutting-down to an extent in the presence of unsubstituted thiophene moieties as discussed above.^[6a-d,8] As shown in Figure 1c, the HOMOs are mostly distributed on the C=C bonds and delocalized along the thiophene units; in contrast, the LUMOs are majorly distributed on the C-C bonds and the S atoms, which

suggests that a hopping-type mechanism dominates hole carrier transport in these materials.^[10]

The thermal properties of 1 and 2 were investigated by thermogravimetric analysis (TGA) and differential scanning calorimetry (DSC) (Table S1). The TGA curves indicated that both compounds possess good thermal stability with the onset weight-loss temperatures of 430 °C for 1 and 434 °C for 2 (Figure S1, Supporting Information). In DSC studies, we observed the typical liquid crystalline characteristics. For 2 as a representative in Figure 2a, the DSC thermogram displayed two endotherm peaks at ~ 135 °C and ~ 160 °C, corresponding to the crystalline-to-liquid crystalline and liquid crystalline-to-isotropic phase transitions, respectively. The polarizing optical microscopy (POM) image of 2 (Figure 2b) showed the characteristic fan-like texture in the temperature ranges of 140–158 and 155–120 °C for the heating and cooling procedures, respectively. This is the typical texture for the smectic liquid crystalline phase, consistent with previous observations in other oligothiophenes and/or polythiophenes.^[6b,6e,6l,6m] The domain size reaches several tens of micrometers.

The X-ray diffraction (XRD), grazing incidence X-ray diffraction (GIXD), atomic

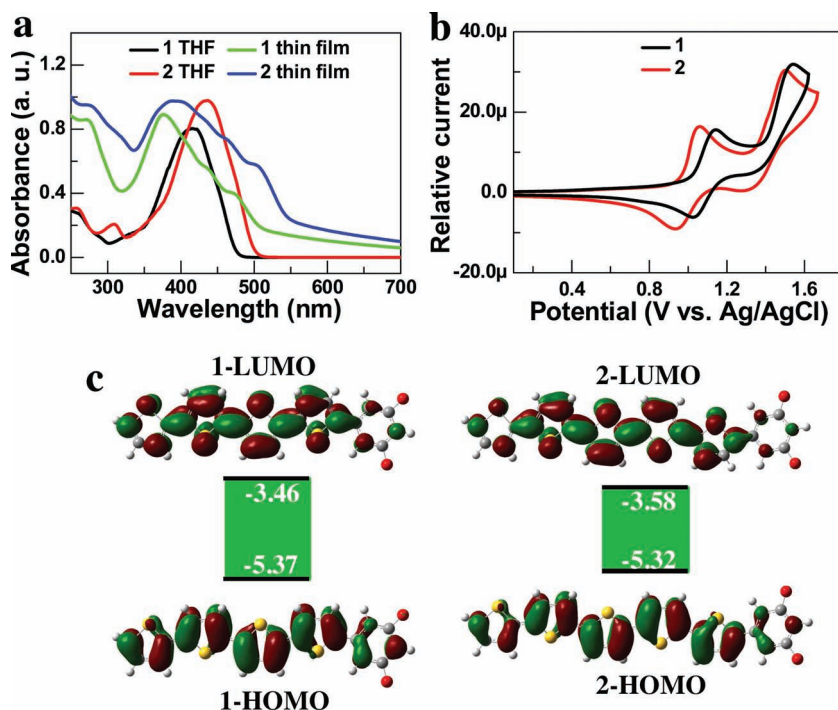


Figure 1. a) The UV-vis absorption spectra of the solutions (10^{-5} M, THF) and annealed thin films (on quartz substrates) of 1 and 2. b) Cyclic voltammograms of 1 and 2 tested in $\text{CH}_2\text{Cl}_2/\text{TBAPF}_6$ solution (scan rate, 50 mV s^{-1}). c) Calculated molecular orbitals (MOs) of 1 and 2.^[10] To clearly show the MOs, we omit the long alkyl side chains.

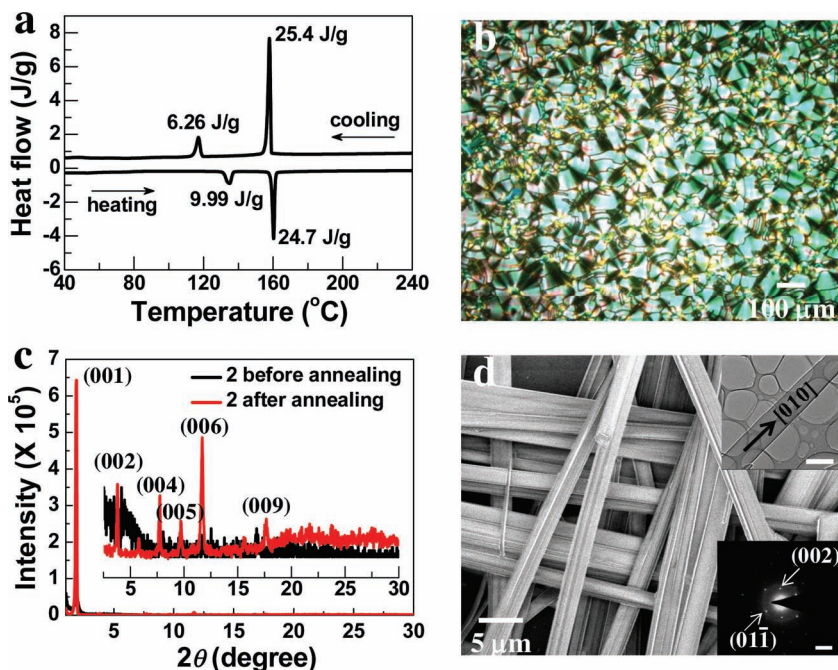


Figure 2. a) The DSC thermogram of **2** at a scan rate of $10\text{ }^{\circ}\text{C min}^{-1}$. b) A POM image of **2** in the temperature ranges of $140\text{--}158$ and $155\text{--}120\text{ }^{\circ}\text{C}$ for the heating and cooling procedures, respectively. c) XRD patterns of a **2** thin film on OTS-treated silicon wafers before and after annealing at $140\text{ }^{\circ}\text{C}$ for 10 min. d) An SEM image of the self-assembled microribbons of **2**. The insets show the TEM image of a **2** single crystal with a scale bar of $2\text{ }\mu\text{m}$ (upper) and the corresponding SEAD pattern with a scale bar of 2 nm^{-1} (lower).

force microscopy (AFM) and scanning tunneling microscopy (STM) were employed to investigate the packing structures and morphologies of the thin films on octadecyltrichlorosilane (OTS)-treated silicon wafers. The XRD patterns of as-cast thin films exhibited a primary diffraction peak at $2\theta = 2.20^{\circ}$ for **1** (Figures S2–S3) and 1.87° for **2** (Figures 2c and S4), revealing the interlayer distance (d -spacing) of $40.2\text{ }\text{\AA}$ for **1** and $47.2\text{ }\text{\AA}$ for **2**, respectively. These are slightly larger than the molecular lengths ($34.8\text{ }\text{\AA}$ for **1** and $38.7\text{ }\text{\AA}$ for **2**) with the fully-extended alkyl groups having all-*anti* conformations, suggesting that intermolecular side-chain interdigitation is formed in the solid state (Scheme 1b).^[6] After thermal annealing at different temperatures the more distinctive, highly crystalline XRD patterns, assigned to the equidistant $(00n)$ reflection family, were observed, which are consistent with the 2D-GIXD patterns (Figures S2–S4, and Figure 2c). The first-order reflection peak with the intensity up to the fifth order became sharper. The appearance of higher-order reflection peaks with negligible π - π stacking peak at $2\theta = \sim 22^{\circ}$ or even its concomitant disappearance proves that the annealing process leads to the formation of highly-ordered lamellar π -stacks that are oriented normal to the substrate surface.^[6a,6f] Thus, both molecules possess the natural capability of self-organizing into highly-crystalline lamella-like layered structure with improved π - π stacking that favors charge transport for improving the device performance, consistent with UV-vis studies and also demonstrated by atomic force microscopic (AFM) investigations where we observed that the crystalline domain size increased after thermal annealing (Figure S5). Further high-resolution

STM images reveal that monolayers of both **1** and **2** show the high-density columnar packing structures (Figures S6–S7), which further proves their packing mode proposed in Scheme 1b.

Organic thin-film transistors with bottom-gate top-contact configurations were fabricated through spin-coating technique under ambient conditions on OTS-modified silicon wafers. The pristine mobilities from as-cast thin films were $\sim 7.6 \times 10^{-3}\text{ cm}^2\text{ V}^{-1}\text{ s}^{-1}$ for **1** and $\sim 0.1\text{ cm}^2\text{ V}^{-1}\text{ s}^{-1}$ for **2**. However, after thermal annealing, the device characteristics improved significantly as summarized in Table 1. The average mobility of **2** increased to as high as $\sim 0.2\text{ cm}^2\text{ V}^{-1}\text{ s}^{-1}$ with an on/off ratio on the order of 10^5 as illustrated in Figure 3 (200 devices), which is very high among the best organic semiconductors based on oligothiophenes or polythiophenes.^[2b,2e] This large improvement should be attributed to the enhanced molecular ordering and π - π stacking induced by thermally-assisted self-assembly of liquid crystals as described above.^[6] It should be noted that all the output characteristics showed almost no contact resistance and good saturation behaviors, which partially results from the fact that the HOMO levels of both compounds match well with the work function of gold electrodes

(5.2 eV). Importantly, the **2** devices are also stable at ambient conditions for at least one month (Figure S11), which may be due to its low-lying HOMO level.

The long alkyl side chains not only increase the molecular solubility allowing for low-cost device fabrication, but also improve the self-assembly ability to form high-quality single crystals, thus offering us the chance to investigate their intrinsic properties. We grew a mat of microribbons from a CHCl_3 solvent via a slow solvent evaporation process. The dimensions of the self-assembled microribbons from **1** and **2** are varying from several tens of microns to $600\text{ }\mu\text{m}$ long, ~ 1 to $5\text{ }\mu\text{m}$ wide, and ~ 40 to 130 nm high (Figures 2d and S2). The transmission electron microscopy (TEM) and selected-area

Table 1. FET properties of thin films and single crystals for semiconductors **1** and **2**.

| Semiconductor type | Average mobility [$\text{cm}^2\text{ V}^{-1}\text{ s}^{-1}$] | $I_{\text{on}}/I_{\text{off}}$ | V_T [V] |
|-------------------------------|--|--------------------------------|-----------|
| 1 thin film | 7.6×10^{-3} | 10^5 | -27 |
| 1 thin film (annealed) | 0.016 | 10^5 | -10 |
| 1 crystal | 0.1 | 10^5 | -25 |
| 2 thin film | 0.1 | 10^5 | -16 |
| 2 thin film (annealed) | 0.2 | 10^5 | -11 |
| 2 crystal | 4.0 | 10^6 | -9 |

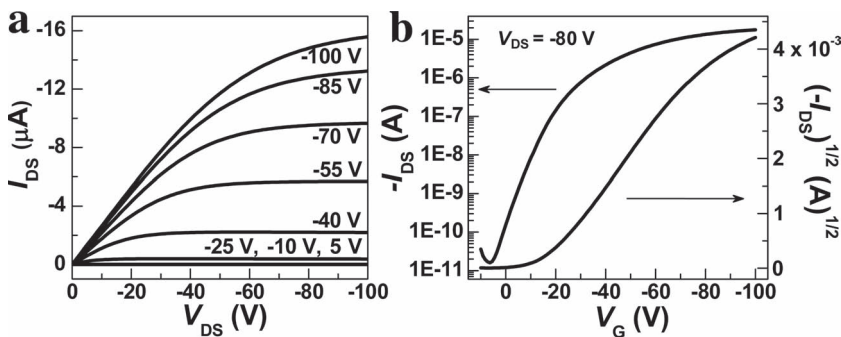


Figure 3. a) Output and b) transfer characteristics of a **2** thin film device after thermal annealing at 140°C for 10 min. $W = 100 \mu\text{m}$, $L = 20 \mu\text{m}$.

electron diffraction (SAED) were used to demonstrate the quality of the self-assembled microribbons (inset in Figure 2d for **2** as representative). The SAED pattern is indexed in combination with the XRD results, showing that the microribbons grows along the π - π stacking (010) direction. The same clear SAED patterns were found in different regions on one microribbon, suggesting the single crystallinity of the 1-dimensional micro-structures.^[2e] To fabricate single crystal transistors, we loaded the self-assembled microribbons by a nondestructive elastomer-based transfer technique onto OTS-treated silicon wafers and then Au leads were deposited by thermal evaporation in vacuum.^[11] Typical transfer and output characteristics of a **2** single crystal are shown in Figures 4a,b. The slight vibrations in both transfer and output curves at high V_{DS} and

V_G were sometimes observed probably due to the contact stability when the thick microribbons were used. Surprisingly, the hole mobility of **2** was calculated to be around $4.5 \text{ cm}^2 \text{ V}^{-1} \text{ s}^{-1}$ with a high on/off ratio on the order of 10^6 and a low threshold voltage (V_T) of $\sim -9 \text{ V}$. Further statistical investigations based on over 60 individual devices reveal an average mobility of $4.0 \text{ cm}^2 \text{ V}^{-1} \text{ s}^{-1}$ with the highest up to $6.2 \text{ cm}^2 \text{ V}^{-1} \text{ s}^{-1}$ (Figure 4c), which ranks the highest among oligothiophene-based semiconducting materials.^[2a-c,2e] These values are also an order of magnitude higher than that of **1** ($0.1 \text{ cm}^2 \text{ V}^{-1} \text{ s}^{-1}$) (Table 1 and Figure S12).

Noticeably, **2** single crystals exhibited the good air stability for at least one month, and the mobilities calculated from both the linear and saturation regimes were almost the same. Interestingly, devices fabricated from either thin films or single crystals of **2** were sensitive to light, showing the reversible and fast photocurrents with a high on/off ratio on the order of $\sim 10^3$ when exposed to light (Figure 4d). Therefore, in combination with the results from thin film characterizations, all the data suggest that **2** is promising in potential applications for organic optoelectronics applications.^[12]

In conclusion, we demonstrated that by rational design of the chemical structure of organic semiconductors for better self-organization ability and proper π -conjugation, excellent OFET performance based on classic thiophene-based semiconductors can be achieved through simple solution processing. Molecule **2** exhibits air-stable thin-film mobilities as high as $0.2 \text{ cm}^2 \text{ V}^{-1} \text{ s}^{-1}$ and an average single-crystal mobility of $4.0 \text{ cm}^2 \text{ V}^{-1} \text{ s}^{-1}$ with the highest up to $6.2 \text{ cm}^2 \text{ V}^{-1} \text{ s}^{-1}$, which ranks the highest among oligothiophene-based semiconductors. These results provide new insights into how to combine molecular engineering and chemical self-assembly with materials fabrication to achieve properties that are desirable for device applications.

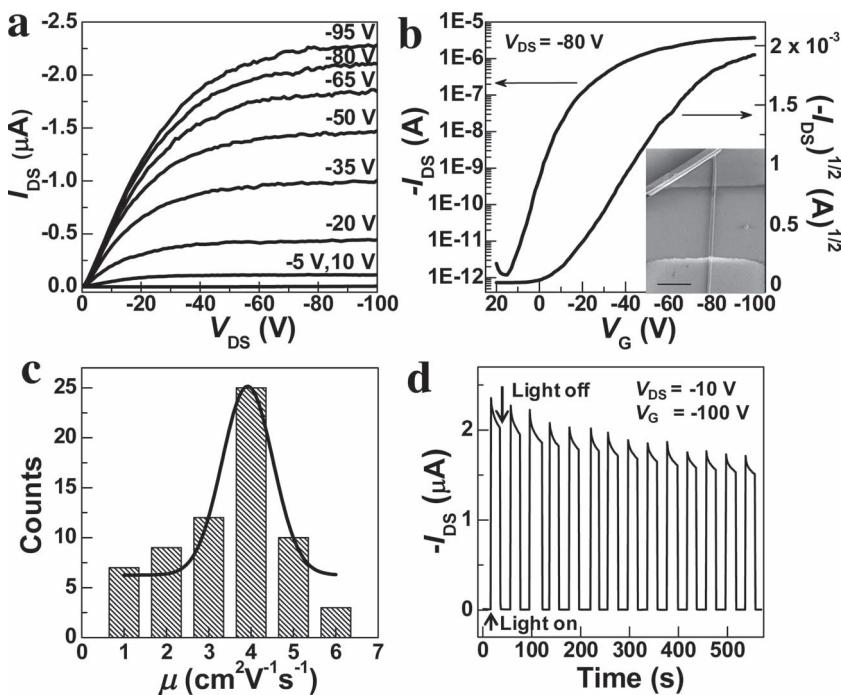


Figure 4. a) Output and b) transfer characteristics of a **2** single crystal device. $W = 1.5 \mu\text{m}$, $L = 23 \mu\text{m}$. Inset shows the SEM image of the device with a scale bar of $10 \mu\text{m}$. c) Statistical mobility distribution of ~ 66 single crystal devices of **2**. d) Photoresponsive behavior of a **2** thin film device.

Supporting Information

Supporting Information is available from the Wiley Online Library or from the author.

Acknowledgements

We thank Prof. Er-Qiang Chen for his helpful discussion. We acknowledge primary financial support from MOST (2009CB623703 and 2012CB921404), and NSFC (20833001, 51121091, and 2007B21).

Received: May 25, 2012

Revised: August 8, 2012

Published online: September 12, 2012

- [1] a) C. D. Dimitrakopoulos, P. R. L. Malenfant, *Adv. Mater.* **2002**, *14*, 99–117; b) J. A. Rogers, Z. Bao, H. E. Katz, A. Dodabalapur, *In Thin-Film Transistors* (Eds: C. R. Kagan, P. Andry), Marcel Dekker, New York, **2003**, 377; c) H. Klauk, *Organic Electronics: Materials, Manufacturing and Applications*, Wiley-VCH Verlag GmbH & Co. KGaA, Weinheim, Germany **2006**.
- [2] a) J. E. Anthony, *Chem. Rev.* **2006**, *106*, 5028–5048; b) A. R. Murphy, J. M. J. Frechet, *Chem. Rev.* **2007**, *107*, 1066–1096; c) J. Zaumseil, H. Sirringhaus, *Chem. Rev.* **2007**, *107*, 1296–1323; d) C. Reese, Z. Bao, *Materials Today* **2007**, *10*, 20–27; e) S. Allard, M. Forster, B. Souharce, H. Thiem, U. Scherf, *Angew. Chem., Int. Ed.* **2008**, *47*, 4070–4098; f) Y. G. Wen, Y. Q. Liu, *Adv. Mater.* **2010**, *22*, 1331–1345; g) R. J. Li, W. P. Hu, Y. Q. Liu, D. B. Zhu, *Acc. Chem. Res.* **2010**, *43*, 529–540; h) H. Usta, A. Facchetti, T. J. Marks, *Acc. Chem. Res.* **2011**, *44*, 501–510; i) B. S. Ong, Y. Wu, Y. Li, P. Liu, H. Pan, *Chem.-Eur. J.* **2008**, *14*, 4766–4778.
- [3] a) Z. Liang, Q. Tang, J. Xu, Q. Miao, *Adv. Mater.* **2011**, *23*, 1535–1539; b) H. S. Tan, N. Mathews, T. Cahyadi, F. R. Zhu, S. G. Mhaisalkar, *Appl. Phys. Lett.* **2009**, *94*, 263303; c) T. W. Kelley, L. D. Boardman, T. D. Dunbar, D. V. Muryes, M. J. Pellerite, T. Y. P. Smith, *J. Phys. Chem. B* **2003**, *107*, 5877–5881; d) M. Kitamura, Y. Arakawa, *J. Phys. Condens. Matter* **2008**, *20*, 184011; e) H. Okamoto, N. Kawasaki, Y. Kaji, Y. Kubozono, A. Fujiwara, M. Yamaji, *J. Am. Chem. Soc.* **2008**, *130*, 10470–10471; f) N. Kawasaki, Y. Kubozono, H. Okamoto, A. Fujiwara, M. Yamaji, *Appl. Phys. Lett.* **2009**, *94*, 043310; g) L. Zhang, L. Tan, Z. H. Wang, W. P. Hu, D. B. Zhu, *Chem. Mater.* **2009**, *21*, 1993–1999; h) T. Yamada, R. Kumai, Y. Takahashi, T. Hasegawa, *J. Mater. Chem.* **2010**, *20*, 5810–5812; i) Y. Takahashi, T. Hasegawa, S. Horiuchi, R. Kumai, Y. Tokura, G. Saito, *Chem. Mater.* **2007**, *19*, 6382–6384; j) K. Takimiya, H. Ebata, K. Sakamoto, T. Izawa, T. Otsubo, Y. Kunugi, *J. Am. Chem. Soc.* **2006**, *128*, 12604–12605; k) T. Yamamoto, K. Takimiya, *J. Am. Chem. Soc.* **2007**, *129*, 2224–2225; l) T. Yamamoto, S. Shinamura, E. Miyazaki, K. Takimiya, *Bull. Chem. Soc. Jpn.* **2010**, *83*, 120–130; m) M. J. Kang, I. Doi, H. Mori, E. Miyazaki, K. Takimiya, M. Ikeda, H. Kuwabara, *Adv. Mater.* **2011**, *23*, 1222–1225; n) K. Niimi, S. Shinamura, I. Osaka, E. Miyazaki, K. Takimiya, *J. Am. Chem. Soc.* **2011**, *133*, 8732–8739.
- [4] a) J. H. Oh, H. W. Lee, S. Mannsfeld, R. M. Stoltenberg, E. Jung, Y. W. Jin, J. M. Kim, J. B. Yoo, Z. N. Bao, *Proc. Natl. Acad. Sci. USA* **2009**, *106*, 6065–6070; b) D. H. Kim, D. Y. Lee, H. S. Lee, W. H. Lee, Y. H. Kim, J. I. Han, K. Cho, *Adv. Mater.* **2007**, *19*, 678–682; c) C. Liu, T. Minari, X. Lu, A. Kumatani, K. Takimiya, K. Tsukagoshi, *Adv. Mater.* **2011**, *23*, 523–526; d) Y. Zhou, T. Lei, L. Wang, J. Pei, Y. Cao, J. Wang, *Adv. Mater.* **2010**, *22*, 1484–1487; e) M. M. Payne, S. R. Parkin, J. E. Anthony, C. C. Kuo, T. N. Jackson, *J. Am. Chem. Soc.* **2005**, *127*, 4986–4987; f) K. Nakayama, Y. Hirose, J. Soeda, M. Yoshizumi, T. Uemura, M. Uno, W. Li, M. J. Kang, M. Yamagishi, Y. Okada, E. Miyazaki, Y. Nakazawa, A. Nakao, K. Takimiya, J. Takeya, *Adv. Mater.* **2011**, *23*, 1626–1629; g) P. Gao, D. Beckmann, H. N. Tsao, X. Feng, V. Enkelmann, M. Baumgarten, W. Pisula, K. Müllen, *Adv. Mater.* **2009**, *21*, 213–216; h) H. Ebata, T. Izawa, E. Miyazaki, K. Takimiya, M. Ikeda, H. Kuwabara, T. Yui, *J. Am. Chem. Soc.* **2007**, *129*, 15732–15733.
- [5] a) T. Izawa, E. Miyazaki, K. Takimiya, *Adv. Mater.* **2008**, *20*, 3388–3392; b) M. Halik, H. Klauk, U. Zschieschang, G. Schmid, S. Ponomarenko, S. Kirchmeyer, W. Weber, *Adv. Mater.* **2003**, *15*, 917–922; c) J. A. Lim, H. S. Lee, W. H. Lee, K. Cho, *Adv. Funct. Mater.* **2009**, *19*, 1515–1525; d) X. Feng, V. Marcon, W. Pisula, M. R. Hansen, J. Kirkpatrick, F. Grozema, D. Andrienko, K. Kremer, K. Muellen, *Nat. Mater.* **2009**, *8*, 421–426; e) L. Zang, Y. Che, J. S. Moore, *Acc. Chem. Res.* **2008**, *41*, 1596–1608.
- [6] a) J. Li, F. Qin, C. M. Li, Q. Bao, M. B. Chan-Park, W. Zhang, J. Qin, B. S. Ong, *Chem. Mater.* **2008**, *20*, 2057–2059; b) B. S. Ong, Y. L. Wu, P. Liu, S. Gardner, *J. Am. Chem. Soc.* **2004**, *126*, 3378–3379; c) Y. N. Li, Y. L. Wu, P. Liu, M. Birau, H. L. Pan, B. S. Ong, *Adv. Mater.* **2006**, *18*, 3029–3032; d) H. L. Pan, Y. N. Li, Y. L. Wu, P. Liu, B. S. Ong, S. P. Zhu, G. Xu, *J. Am. Chem. Soc.* **2007**, *129*, 4112–4113; e) I. McCulloch, M. Heeney, C. Bailey, K. Genevicius, I. Macdonald, M. Shkunov, D. Sparrowe, S. Tierney, R. Wagner, W. M. Zhang, M. L. Chabinc, R. J. Kline, M. D. McGehee, M. F. Toney, *Nat. Mater.* **2006**, *5*, 328–333; f) F. P. Zhang, M. Funahashi, N. Tamaoki, *Org. Electron.* **2009**, *10*, 73–84; g) M. Funahashi, J. I. Hanna, *Adv. Mater.* **2005**, *17*, 594–598; h) T. Fujiwara, J. Locklin, Z. N. Bao, *Appl. Phys. Lett.* **2007**, *90*, 232108; i) M. Melucci, L. Favaretto, C. Bettini, M. Gazzano, N. Camaioni, P. Maccagnani, P. Ostojka, M. Monari, G. Barbarella, *Chem.-Eur. J.* **2007**, *13*, 10046–10054; j) A. van Breemen, P. T. Herwig, C. H. T. Chlon, J. Sweelssen, H. F. M. Schoo, S. Setayesh, W. M. Hardeman, C. A. Martin, D. M. de Leeuw, J. J. P. Valetton, C. W. M. Bastiaansen, D. J. Broer, A. R. Popa-Merticar, S. C. J. Meskers, *J. Am. Chem. Soc.* **2006**, *128*, 2336–2345; k) M. Katsuhara, I. Aoyagi, H. Nakajima, T. Mori, T. Kambayashi, M. Ofuji, Y. Takanishi, K. Ishikawa, H. Takezoe, H. Hosono, *Synth. Met.* **2005**, *149*, 219–223; l) A. Matsui, M. Funahashi, T. Tsuji, T. Kato, *Chem.-Eur. J.* **2010**, *16*, 13465–13472; m) T. Yasuda, H. Ooi, J. Morita, Y. Akama, K. Minoura, M. Funahashi, T. Shimomuro, T. Kato, *Adv. Funct. Mater.* **2009**, *19*, 411–419.
- [7] a) S. M. Zhang, Y. L. Guo, Y. J. Zhang, R. G. Liu, Q. K. Li, X. W. Zhan, Y. Q. Liu, W. P. Hu, *Chem. Commun.* **2010**, *46*, 2841–2843; b) Y. Zhou, T. Lei, L. Wang, J. Pei, Y. Cao, J. Wang, *Adv. Mater.* **2010**, *22*, 1484–1487; c) Y. Zhou, W.-J. Liu, Y. Ma, H. Wang, L. Qi, Y. Cao, J. Wang, J. Pei, *J. Am. Chem. Soc.* **2007**, *129*, 12386–12387.
- [8] a) I. McCulloch, C. Bailey, M. Giles, M. Heeney, I. Love, M. Shkunov, D. Sparrowe, S. Tierney, *Chem. Mater.* **2005**, *17*, 1381–1385; b) M. Heeney, C. Bailey, K. Genevicius, M. Shkunov, D. Sparrowe, S. Tierney, I. McCulloch, *J. Am. Chem. Soc.* **2005**, *127*, 1078–1079.
- [9] a) A. Schenning, A. F. M. Kilbinger, F. Biscarini, M. Cavallini, H. J. Cooper, P. J. Derrick, W. J. Feast, R. Lazzaroni, P. Leclere, L. A. McDonnell, E. W. Meijer, S. C. J. Meskers, *J. Am. Chem. Soc.* **2002**, *124*, 1269–1275; b) M. Muccini, E. Lunedi, C. Taliani, D. Beljonne, J. Cornil, J. L. Bredas, *J. Chem. Phys.* **1998**, *109*, 10513–10520.
- [10] The details of the theoretical calculations can be found in the Supporting Information. G. R. Hutchison, M. A. Ratner, T. J. Marks, *J. Am. Chem. Soc.* **2005**, *127*, 2339–2350.
- [11] S. X. Xiao, J. Y. Tang, T. Beetz, X. F. Guo, N. Tremblay, T. Siegrist, Y. M. Zhu, M. Steigerwald, C. Nuckolls, *J. Am. Chem. Soc.* **2006**, *128*, 10700–10701.
- [12] a) H. Sirringhaus, N. Tessler, R. H. Friend, *Science* **1998**, *280*, 1741–1744; b) X. Gong, M. Tong, Y. Xia, W. Cai, J. S. Moon, Y. Cao, G. Yu, C.-L. Shieh, B. Nilsson, A. J. Heeger, *Science* **2009**, *325*, 1665–1667.